Structural and magnetic properties of Fe thin films on $Cu_{90}Au_{10}(001)$

S. S. Kang,* W. Kuch,† and J. Kirschner
Max-Planck-Institut für Mikrostrukturphysik, Weinberg 2, D-06120 Halle, Germany
(Received 3 August 2000; published 11 December 2000)

A series of Fe thin films with thicknesses ranging from 1 monolayer (ML) to 30 ML was deposited on a $Cu_{90}Au_{10}$ (001) substrate ($a=3.66$ Å) at room temperature. Structural properties were investigated by low-energy electron diffraction (LEED). From intensity vs energy [I(E)] measurements of the specular LEED reflection, three different structural phases were observed. The first phase at low Fe thicknesses (<4 ML) is a tetragonally expanded fcc phase (fct) with an interlayer distance $a_\perp$ above 1.90 Å. The second phase at Fe thicknesses between 4 and 10 ML is associated with an interlayer distance $a_\perp \approx 1.76$ Å. With further increasing Fe thickness (>10 ML), the third phase, a bcc(011) structure with $a_\perp \approx 2.03$ Å, occurs. The magnetic properties were studied by *in situ* magneto-optical Kerr effect (MOKE). It was found that the Fe films of the first and third phase have a high-spin ferromagnetic moment, while they exhibit a low net magnetic moment in the second phase. The observed structural and magnetic phases are thus similar to the Fe/Cu(001) system. The direction of the easy magnetic axis in $Fe/Cu_{90}Au_{10}$ is perpendicular to the film plane only at thicknesses below 2 ML, where a spin-reorientation transition from perpendicular-to-the-film-plane to in-plane with increasing film thickness has been found. The origin of perpendicular magnetization is discussed.

DOI: 10.1103/PhysRevB.63.024401 PACS number(s): 75.70.Ak, 75.50.Bb, 68.55.−a

I. INTRODUCTION

The growth of epitaxial thin films of ferromagnetic material on nonmagnetic substrates under ultrahigh vacuum conditions has long been a subject of interest. By deposition of ultrathin films it is possible to stabilize new materials with properties that deviate from the corresponding bulk crystals.[1] To tailor films with specific properties, the knowledge about the correlation between the magnetic and structural properties is required. Ultrathin Fe films are particularly suited for an investigation of this correlation, because Fe can exist in a ferromagnetic (FM) bcc, FM fcc or antiferromagnetic (AF) fcc modification.[2–6] For example, varying the film thickness or changing the growth temperature in the Fe/Cu(100) system, a face centered tetragonal (fct) to fcc structural evolution[7,8] has been shown to be responsible for a magnetic phase transition from a ferromagnetic to a nonferromagnetic (antiferromagnetic or paramagnetic) phase.[9–12] The structural evolution gives rise to a change of the lattice parameter, leading to the magnetic phase transition. This behavior is mainly attributed to the critical value of the Cu lattice constant (3.61 Å), which is exactly the value for which a transition between a high-spin and a low-spin ferromagnetic state of fcc Fe is predicted.[3–5] By using alternative substrates such as Cu_3Au,[13] which has a larger lattice constant of 3.75 Å, the fcc-like Fe films exhibit only a ferromagnetic phase, independently of the growth temperature.[13,14]

In order to investigate more systematically the influence of the lattice strain induced by the substrate on epitaxial ultrathin fcc-like Fe films, more experimental data for Fe films grown on a substrate with a lattice parameter different from that of Cu(001) and $Cu_3Au(001)$ would be desirable. One way to achieve that is to use a single crystal of a CuAu alloy with an intermediate composition. At 90 atomic percent Cu the lattice parameter is 3.66 Å,[15] and lies thus in between the lattice parameters of Cu and Cu_3Au. The study of Fe films on $Cu_{90}Au_{10}(001)$ should thus broaden the knowledge about the dependence of structural and magnetic properties of fcc-like Fe films on the substrate lattice parameter.

In this paper, we present a combined study of growth, structure, and magnetism of Fe films on a $Cu_{90}Au_{10}(001)$ single crystal substrate, using low energy electron diffraction (LEED), medium energy electron diffraction (MEED) during film growth, and magneto-optical Kerr effect (MOKE) measurements. The simultaneous determination of structural and magnetic properties has the advantage that it allows to assign the observed structural phases in that system to the corresponding magnetic behavior. The experiment is aimed to contribute to a systematic understanding of the influence of the in-plane strain on the structural and magnetic properties of fcc Fe films.

II. EXPERIMENTAL TECHNIQUES

The experiments were performed in an ultrahigh-vacuum chamber designed for measurements of the magnetism and structure of ultrathin films. The chamber is equipped with facilities for LEED, Auger electron spectroscopy (AES), MOKE, and thin film growth. Details can be found elsewhere.[13] A face to face arrangement of the LEED system and the AES system permits the MEED measurement in a grazing incidence geometry, by recording the intensity of the specularly reflected electron beam displayed on the LEED fluorescent screen. To monitor the process of film growth, MEED with an incidence angle of less than 5° was employed during the evaporation of iron. The $Cu_{90}Au_{10}(001)$ substrate was cleaned *in situ* by repeated cycles of Ar^+ sputtering and subsequent annealing at 800 K, until there was a sharp and low-background LEED pattern. Surface impurities were below the AES detection limit ($\approx 1\%$). Fe films were deposited with the substrate at room temperature from an Fe wire of high purity (99.99%), heated by electron bombardment. The Fe thickness was determined by MEED and AES. The pressure during Fe deposition was kept below 3

$\times 10^{-8}$ Pa at an evaporation rate of about 1 atomic monolayer (ML)/min. During the measurements it was below 1.5 $\times 10^{-8}$ Pa. The magnetic properties of the films were studied by *in situ* MOKE measurements. For the MOKE measurements, two He–Ne lasers with photoelastic modulators and one photodiode as light detector were employed. The lasers and the detector were arranged in such a way that both the polar and the longitudinal Kerr signals can be measured by just rotating the sample about its vertical axis without any rearrangement of the optical elements.[16] Such a setup allows a reliable measurement of spin-reorientation transitions, which needs quasi-simultaneous measurement of both the perpendicular and in-plane Kerr signal. Longitudinal MOKE measurements were taken in the [100] azimuth. For the structural investigation of the films, the intensity of the LEED specular beam vs electron energy $[I(E)]$ was measured. A full interpretation of a LEED I(E) curve is, in general, more involved than can be done within a kinematic analysis. Information on the average vertical interlayer distance, however, can be extracted from the LEED I(E) curves taken for the (00) diffraction beam, by considering a constructive interference condition for the electron wave (Bragg condition) within the kinematic analysis. The vertical interlayer distance $a_\perp$ can then be expressed as[17,18]

$$a_\perp = \frac{n\pi\hbar}{\sin\theta\sqrt{2m_e(E_p(n)-V_0)}}. \tag{1}$$

Here, the integer n is the order of the corresponding interference peak, $E_p(n)$ the primary energy of the electron of that peak, V_0 is the additional energy shift due to the average inner potential in the crystal, m_e is the electron mass, and θ is the incident angle with respect to the sample surface. $a_\perp$ is determined by a linear regression of $E_p(n)$ vs. n^2, where V_0 was treated as a second fit parameter. This method has been successfully applied to the Fe/Cu(001) system[19,20] for monitoring the average vertical interlayer distance as a function of temperature.

III. RESULTS

A. Structure

Figure 1 shows the LEED patterns of (a) the clean ordered $Cu_{90}Au_{10}(001)$ substrate and (b) after 7 ML Fe deposition. The LEED picture of the substrate shows sharp spots and a clear c(2×2) reconstruction. This indicates that the $Cu_{90}Au_{10}$ substrate surface is well crystallized, and flat within the transfer width of the LEED system ($\approx$100 Å). The c(2×2) superstructure is very similar to that observed on ordered $Cu_3Au(001)$,[14,18] and could be an indication for Au enrichment on the surface. The diffraction pattern of 7 ML Fe/$Cu_{90}Au_{10}(001)$ [Fig. 1(b)] reveals a p(1×1) structure with spots at the same positions as the (10) spots of the substrate, indicating a growth of the Fe film in an fcc-like structure. The $(\frac{1}{2}\frac{1}{2})$ superstructure spots, which were observed for the clean $Cu_{90}Au_{10}(001)$ substrate, have vanished. Within the limited accuracy of the LEED spot position determination of about 3%, a pseudomorphic growth can be

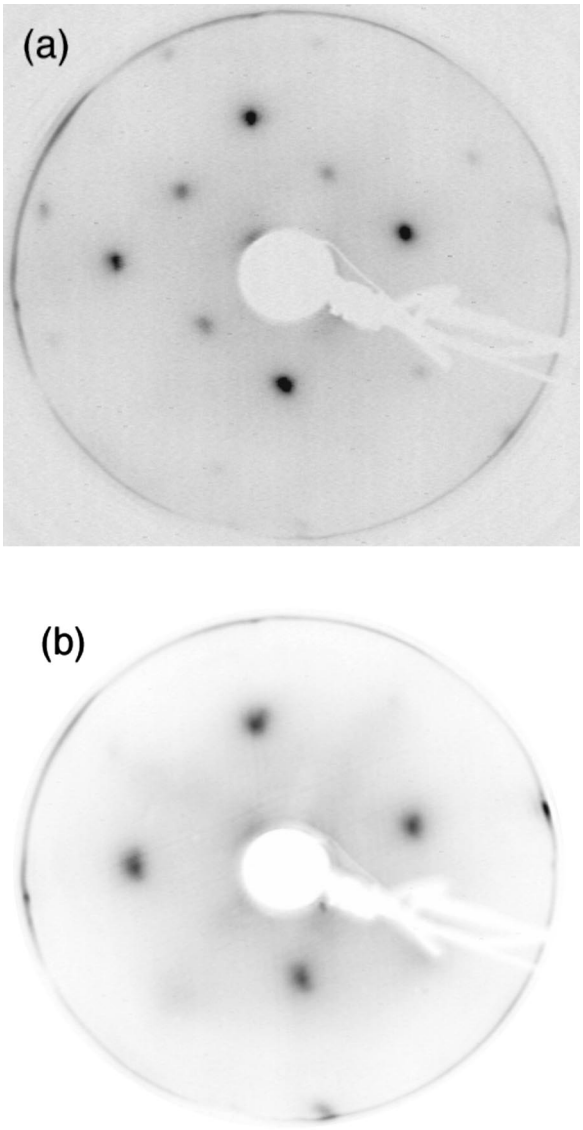

FIG. 1. LEED patterns for 136 eV electron energy of (a) the $Cu_{90}Au_{10}(001)$ substrate, and (b) after deposition of 7 ML Fe.

stated. In contrast to the Fe/Cu(100) system, where (4×1) and (5×1) superstructures were found in the coverage regime of the perpendicular ferromagnetic phase,[7,10] no superstructure due to a reconstruction of the Fe layer could be observed in Fe/$Cu_{90}Au_{10}(001)$ at all thicknesses under investigation. This is similar to the findings in Fe/$Cu_3Au(001)$.[18] The absence of a regular reconstruction as indicated in the LEED pattern may thus be attributed to the higher tensile strain due to the larger lattice mismatch in our system, in accordance with the result from $Fe_xCo_{1-x}/Cu(001)$, where reconstructions of the FeCo film were only observed for compressive strain.[21]

For the characterization of the growth, the MEED intensity of the (00) spot was measured during Fe deposition. Figure 2 shows MEED data for the growth of 12 ML Fe on $Cu_{90}Au_{10}(001)$. The intensity shows well-defined oscillations up to a film thickness of about 10 ML. They are characteristic of a layer-by-layer growth mode. In addition, a

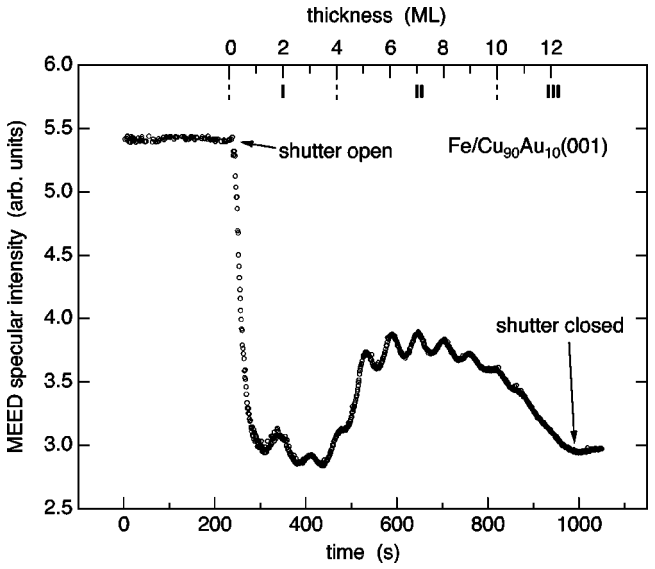

FIG. 2. MEED specular beam intensity as a function of time during the deposition of 12 ML Fe on $Cu_{90}Au_{10}(001)$. The corresponding film thickness is given at the upper axis. Three qualitatively different thickness regions are labeled I, II, and III.

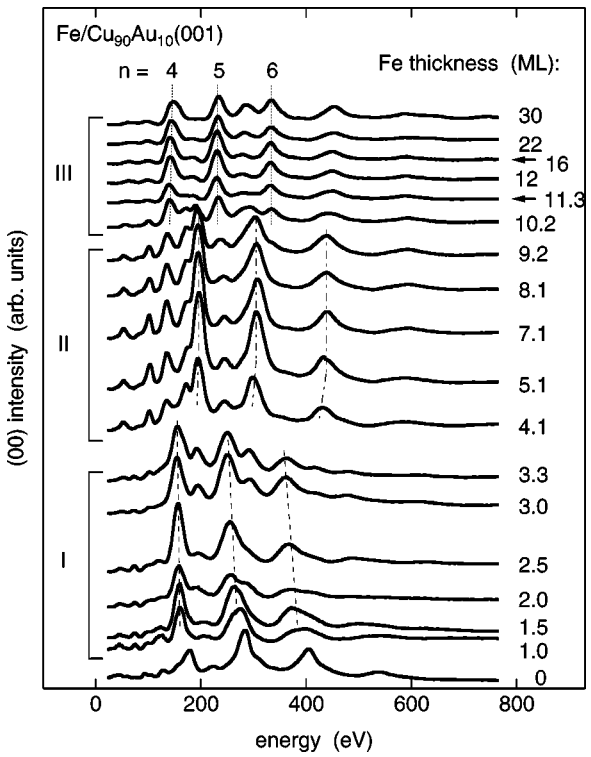

FIG. 3. Intensity vs energy $[I(E)]$ curves of the LEED (00) specular beam for the clean $Cu_{90}Au_{10}(001)$ substrate (bottom-most curve), and for $Fe/Cu_{90}Au_{10}(001)$ films of various Fe thicknesses, as indicated on the right hand side, measured at room temperature. Three distinctly different Fe thickness regimes, labeled I, II, and III on the left hand side, can be distinguished by different types of $I(E)$ curves. The dashed, dash–dotted, and dotted lines denote the corresponding sequences of kinematic peak maxima. The numbers at the top give the scattering order for the sequence of peak maxima at high Fe thicknesses.

distinct change of the MEED intensity between thicknesses below and above ≈ 4 ML is observed. The MEED intensity is not only influenced by the morphology of the film surface during growth, but also by the film structure.[22,23] The increase in MEED intensity at ≈ 4 ML Fe thickness could indicate a structural transition in the films, like in Fe/Cu(001), where similar MEED curves have been observed.[9,10,21,24,25] The variation of the MEED intensity is also accompanied by a distinct change of the MEED pattern. At a thickness above 4 ML, a reduction of the spot intensity and an increase in spot size was observed.

More quantitative structural information can be obtained from LEED $I(E)$ measurements. Figure 3 contains a compilation of LEED I(E) curves of the (00) diffraction spot taken at room temperature for the clean $Cu_{90}Au_{10}(001)$ substrate (bottommost curve) and for Fe films of various thicknesses d_{Fe}, as indicated on the right hand side. Three thickness regions with clearly different shape of the $I(E)$ curves can be easily distinguished from looking at the curves of Fig. 3, as indicated on the left hand side. The dashed, dash–dotted, and dotted lines highlight three different peak sequences with equal $\sqrt{E}$ separation, which correspond to three different structural phases. The indices at the top of the figure denote the integer number of the electron wavelength associated with a constructive interference as shown in Eq. (1) in Sec. II. The first peak sequence (dashed lines) observed for Fe films up to 4 ML thickness is found at lower energies than the corresponding sequence of the clean substrate. It has to be attributed to a structural phase of Fe with an expanded vertical interlayer distance. With increasing Fe thickness, the intensity of the first peak sequence decreases. At 4 ML Fe thickness, the second peak sequence appears (dash–dotted lines), which is observed up to ≈ 10 ML thickness. The energetic positions of the peaks of this sequence indicate a structural phase with a reduced interlayer distance compared to that of the substrate. The third peak sequence (dotted lines) occurs in the films with thickness >10 ML. The interpretation of this sequence as belonging to a structure with a distinctly higher vertical interlayer distance as that of the substrate, as labeled at the top of Fig. 3, is consistent with a (110) oriented bcc phase of Fe, as will be shown below. A closer examination of the curves reveals that films of 4–5 ML thickness are characterized by a coexistence of the first and the second structural phase. At 9–10 ML, the films exhibit signs of a coexistence of the second and third phase.

Values for the average vertical atomic interlayer distance $a_\perp$ for each film thickness can be extracted from the energetic positions of the kinematic peaks in the LEED $I(E)$ curves of Fig. 3 according to Eq. (1). $a_\perp$ is obtained as the slope of plots of the peak energy $E(n)$ vs n^2. Such plots for 3, 7, and 30 ML representing the three different structural phases are presented in the inset of Fig. 4. The excellent agreement with Eq. (1) demonstrates the validity of the assignment of n. The values of $a_\perp$ for all Fe thicknesses investigated are shown in Fig. 4 as a function of film thickness. The horizontal dotted line indicates the experimental value for $a_\perp$ of the clean substrate (1.855 Å). This is slightly larger than 1.83 Å, which would be expected from the bulk

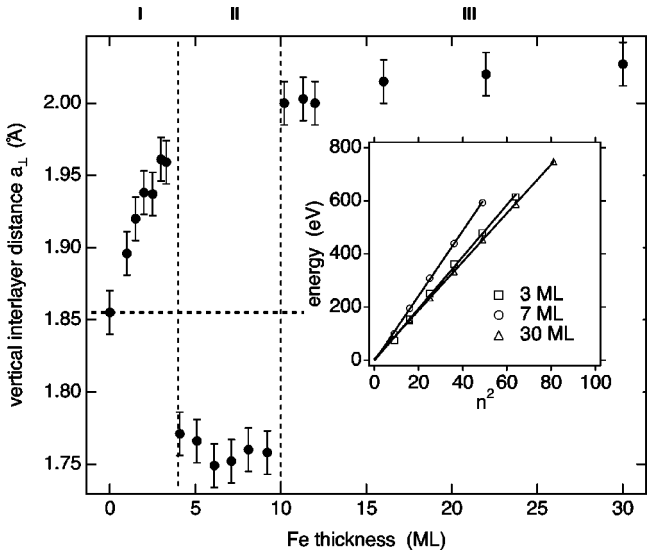

FIG. 4. Average vertical interlayer distances $a_\perp$ extracted from the kinematic peak sequences in the I(E) curves of Fig. 3. The value of $a_\perp$ that was measured for the $Cu_{90}Au_{10}(001)$ substrate is highlighted by the dotted horizontal line. The inset shows representative examples of the kinematic analysis of the peak sequences of Fig. 3. Energy positions of these peaks are plotted vs the square of the corresponding scattering order n for three Fe thicknesses of 3, 7, and 30 ML, representative of the three different structural regions seen in Fig. 3 and labeled I, II, and III.

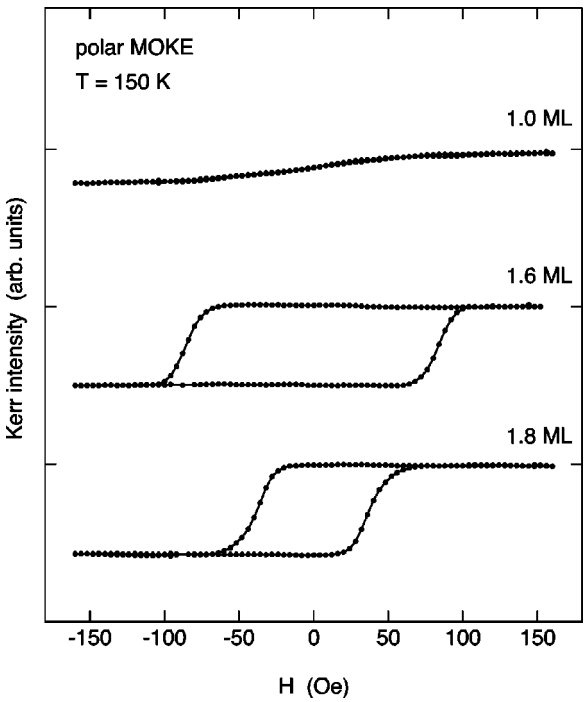

FIG. 5. Polar MOKE loops for $Fe/Cu_{90}Au_{10}(001)$ films with Fe thicknesses of 1.0, 1.6, and 1.8 ML at 150 K.

lattice constant. This discrepancy may be due to a systematic error in the kinematic analysis of the LEED $I(E)$ curves, or to a surface relaxation of the interlayer lattice spacing of $Cu_{90}Au_{10}(001)$. Values increasing from 1.90 to 1.96 Å with thickness are found for the first peak sequence of Fe on $Cu_{90}Au_{10}(001)$, labeled I in Fig. 4. This is significantly larger than the substrate layer spacing. We attribute this, similar to Fe/Cu(001) (Refs. 7 and 10) and $Fe/Cu_3Au(001)$ (Refs. 14 and 18) to a vertically expanded fct phase of Fe. The increase of $a_\perp$ with Fe thickness could be due to the influence of the substrate $a_\perp$ in the LEED $I(E)$ curves at very low Fe thicknesses. A reduction of the Fe lateral lattice spacing by less than 3% by the occurrence of misfit dislocations can also not be ruled out. For the second peak sequence (II), $a_\perp$ is around 1.76 Å, i.e., smaller than that of the substrate, and close to the interlayer distance of (001)-oriented fcc Fe/Cu(001).[8] For a pseudomorphic lateral lattice spacing this would mean a contraction in vertical direction compared to the substrate fcc lattice. We attribute this phase thus to a vertically compressed fct phase of Fe. Increasing the Fe thickness beyond 10 ML, $a_\perp$ extracted from the third peak sequence (III) approaches an interlayer distance of 2.03 Å. This value is quite close to the interlayer spacing of bulk bcc Fe in the $\langle 110 \rangle$ direction (2.066 Å). We conclude thus that the third phase, like in thick Fe films on Cu(001),[26,27] consists mainly of (011) oriented bcc Fe.

B. Magnetic properties

The magnetic properties of all films were investigated using *in-situ* MOKE. Figure 5 shows the development of the MOKE loops in polar geometry for 1.0, 1.6, and 1.8 ML Fe films at 150 K. A significant MOKE signal was first detected for a thickness of 1 ML, with the intensity linearly proportional to the applied magnetic field. The lacking of hysteresis indicates that the ferromagnetic phase is not yet developed at that temperature. The magnetization curve hints towards the presence of superparamagnetism. Increasing the Fe thickness up to 1.6 or 1.8 ML, the loops in Fig. 5 clearly show hysteresis, demonstrating the onset of ferromagnetism. For films less than 2 ML, the strong polar Kerr signal indicates an easy direction of the magnetization perpendicular to the film plane.

Figure 6 shows longitudinal MOKE curves for 1.0, 1.6, 3.3, 5.1, 8.1, and 16 ML Fe films. For 1 ML the longitudinal MOKE intensity is linearly proportional to the applied magnetic field. Between $\approx$1.5 and 2 ML the Fe films can be saturated in both the longitudinal and polar geometry by fields of 200 Oe. The curve for 1.6 ML in Fig. 5 shows an in-plane magnetic signal without hysteresis, indicative for a hard axis of magnetization. For Fe thicknesses of 3.3 ML and higher the MOKE curves show that the easy axis of magnetization is in-plane. For ultrathin ferromagnetic films, the Kerr effect initially depends linearly on the thickness if the magnetization is thickness-independent.[28] But in Fig. 6, the Kerr signal of the saturation magnetization is about the same for 3.3, 5.1, and 8.1 ML. At 16 ML it is more than four times higher than at 8.1 ML. The detailed thickness dependence of the longitudinal saturation Kerr intensity is plotted in Fig. 7. The MOKE intensity increases sharply with thickness in the range of 1.6–3.3 ML, just after the onset of ferromagnetism. Extrapolation of those points towards zero yields an ordinate intersection close to zero, which means that there is no significant amount of magnetically dead lay-

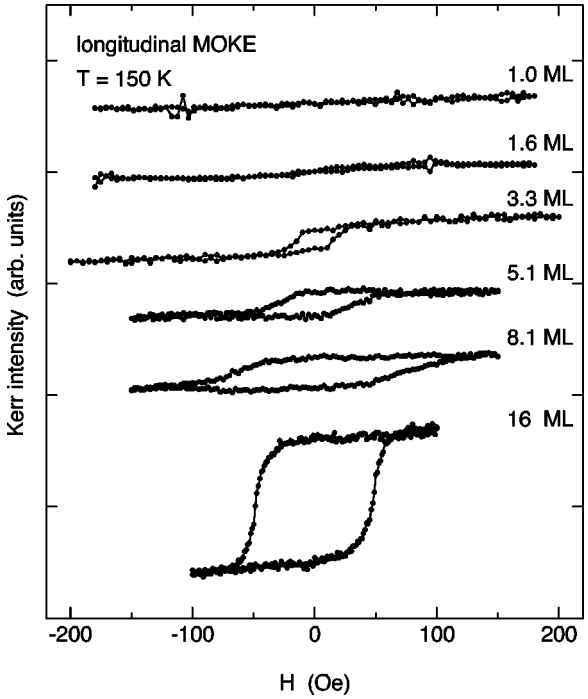

FIG. 6. Longitudinal MOKE loops for $Fe/Cu_{90}Au_{10}(001)$ films with Fe thicknesses of 1.0, 1.6, 3.3, 5.1, 8.1, and 16 ML at 150 K.

ers between the interface of the Fe film and the $Cu_{90}Au_{10}(001)$ substrate. The Kerr intensity increases linearly with Fe thickness up to 3.3 ML, which is related to the growth of a homogeneous ferromagnetic film in phase I. Above 3.3 ML the Kerr intensity decreases, following the structural phase transition from the expanded to the compressed fct-Fe film. The reduction of the Kerr intensity is due to the presence of either paramagnetic or antiferromagnetic Fe in that phase. The Kerr intensity is almost constant in the second phase (II). At an Fe thickness of 10 ML, where the bcc(011) oriented Fe appears, the Kerr intensity increases again rapidly. This can be understood by the dominating contribution of ferromagnetic bcc-Fe to the magnetization.

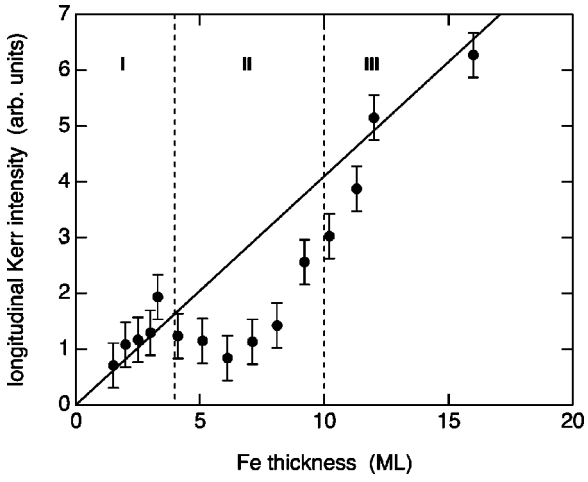

FIG. 7. Thickness dependence of the longitudinal MOKE intensity. The three structurally different thickness regions are indicated and labeled I, II, and III.

IV. DISCUSSION AND CONCLUSION

We observed three structurally and magnetically different phases in $Fe/Cu_{90}Au_{10}(001)$. Up to 4 ML Fe thickness ferromagnetism and high atomic interlayer distances in an fcc-like structure are observed (phase I). A second phase (II) can be identified between ≈ 4 and 10 ML Fe thickness. It is partly nonferromagnetic. The structure is also fcc-like, with lower interlayer distances. At Fe thicknesses above 10 ML phase III, a ferromagnetic phase with bcc(011) structure is found. The presence of these three phases in $Fe/Cu_{90}Au_{10}(001)$ qualitatively resembles the respective phases found in Fe/Cu(001) at very similar thicknesses. The 1.4% larger lattice constant of $Cu_{90}Au_{10}$ compared to Cu seems to have no strong influence on the structural and magnetic properties of the Fe films. On the other hand, in $Fe/Cu_3Au(001)$, only phase I was found in a similar thickness interval, followed by an immediate conversion of the Fe films to (001) oriented bcc-Fe.[14,18]

As mentioned in Sec. III A, the observed superstructure in the LEED image of the clean sample [Fig. 1(a)] could be an indication for Au enrichment at the surface. The measured vertical interlayer distance, however, is only slightly larger (within the systematic error of the method) than expected for bulk $Cu_{90}Au_{10}$, and clearly different from the values obtained for Cu or Cu_3Au. We conclude thus that no significant deviation of the surface lattice constant from the bulk occurs.

Interesting is a comparison of the vertical interlayer distances of phase I in the three systems, whereas the interlayer spacing at small Fe thicknesses in Fe/Cu(001) was determined by a full-dynamical LEED analysis as varying between 1.85 and 1.90 Å,[7] in $Fe/Cu_{90}Au_{10}(001)$ we find even higher values ranging between 1.90 and 1.96 Å. In $Fe/Cu_3Au(001)$ very similar values of 1.90–1.94 Å were found.[18] This might be puzzling in view of an elastic strain picture, since it is then expected that the larger lateral lattice distances of $Cu_{90}Au_{10}(001)$ or $Cu_3Au(001)$ would lead to a reduction of the vertical lattice distance of Fe. One has to consider the possibility that in the purely kinematic LEED analysis of the present data and of Ref. 18 a certain systematic error might be present. A previous kinematic LEED analysis of Fe/Cu(001) (Ref. 20) resulted in values of the average Fe interlayer spacing that were systematically higher by 0.01–0.03 Å than the corresponding values of a fully dynamical tensor LEED study.[7,8] Considering further the $a_\perp$ value we find for the clean substrate, and keeping in mind that no superstructure indicating a vertical buckling of the Fe films was observed, we think that $a_\perp$ is systematically overestimated by not more than 1.5%.

A possible explanation of this behavior of $a_\perp$ could be a noncubic, i.e., tetragonal ground state of fcc-like Fe, as suggested by Marcus *et al.*[29] Another point that we have to consider in this context is that we cannot rule out completely a nonpseudomorphic reduced lateral lattice spacing of the Fe films. In any case we can conclude that the rather large lattice spacing of 1.90 Å or higher of ferromagnetic (''high spin'') fcc-like Fe does not result from lateral tensile strain from the substrate.

The formation of nonferromagnetic fcc-like Fe [phase II

in Fe/$Cu_{90}Au_{10}$(001) and Fe/Cu(001)] seems to be suppressed above a certain critical substrate lattice parameter, which must be in between the one of $Cu_{90}Au_{10}$ and the one of Cu_3Au, i.e., between 3.66 and 3.75 Å. Also, in phase II a close similarity of the vertical interlayer distances of Fe/$Cu_{90}Au_{10}$(001) (1.76 Å) and Fe/Cu(001) (between 1.76 and 1.78 Å[8]) can be stated. The same discussion as before holds for that phase. Experimental evidence for a nonpseudomorphic in-plane lattice match of Fe on Cu(001) in that phase has already been claimed by Müller *et al.*[8]

Another point is the origin of the perpendicular anisotropy in the fcc-like Fe films. The critical thickness $t_c < 2.0$ ML for the spin-reorientation transition from perpendicular to in-plane magnetization in our system is less than the one in Fe/Cu(001) and Fe/Cu_3Au(001), where t_c is 11 and 3.5 ML, respectively.[9,14] Commonly, the magnetocrystalline surface anisotropy, which is assumed to be responsible for the existence of the perpendicular magnetization in ultrathin Fe films, is due to the broken symmetry of the crystalline structure at the surface and at the interface, and is consequently very sensitive to the quality of the surface or interface. A poor crystalline structure with dislocations and defects at the surface (interface) could obscure the symmetry character of the surface, and consequently may drastically reduce the magnetocrystalline perpendicular surface anisotropy. However, also other sources of the perpendicular magnetization than the magnetocrystalline surface anisotropy have been discussed. Fowler *et al.* have reported that for Fe/Cu(001) also a perpendicular volume anisotropy is found to have a crucial contribution to the resulting out-of-plane easy axis.[30] This perpendicular volume anisotropy is assumed, according to Ref. 30, to be caused by the lattice distortion (expansion) normal to the film surface. Nevertheless, an estimate of this perpendicular volume anisotropy within a magnetoelastic model gives a value one order of magnitude smaller than the measured one.[30] It has been observed, however, that in ultrathin films the magnetoelastic constants can be very different from the corresponding bulk values.[31] In the absence of a direct measurement of the magnetic anisotropy constant for fcc-like Fe/$Cu_{90}Au_{10}$(001), we cannot quantitatively confirm the presence of such a perpendicular volume anisotropy, which should, in principle, also exist in our system due to the lattice expansion along the sample normal.

In conclusion, the structural and magnetic properties of Fe films, epitaxially grown on $Cu_{90}Au_{10}$(001), were investigated by using MEED, LEED $I(E)$, and MOKE measurements. Varying the Fe thickness between 1 and 30 ML, three different structural phases were observed. For small Fe thicknesses below 4 ML the Fe films exist in a tetragonally expanded fcc-like phase. With increasing Fe thickness, a tetragonally compressed fcc-like structure occurs. At Fe thicknesses above 10 ML, the films exhibit an fcc–bcc structural transition. Three distinct magnetic phases associated to the structural phases of the Fe films have been identified: the expanded fcc-like films and the bcc films are ferromagnetic with comparable moments, while the compressed fcc-like films show a lower net magnetic moment. Furthermore, a spin-reorientation transition of the magnetic easy axis from out-of-plane to in-plane has been found for the fct films at about 2 ML Fe thickness.

ACKNOWLEDGMENTS

The authors would like to thank B. Zada for her expert technical support. S.S.K. thanks the Max-Planck-Society for a stipend.

*Present address: RISM, Tohoku University, Katahira 2-1-1, Aoba-Ku, Sendai 980-8577, Japan.

†Author to whom correspondence should be addressed. FAX: +49-30-6392-4984. Electronic address: kuch@bessy.de

[1] G.A. Prinz, J. Magn. Magn. Mater. **100**, 469 (1991).

[2] See, for example, U. Gradmann, in *Magnetism in Ultrathin Transition Metal Films*, edited by K. H. J. Buschow (Elsevier Science, Amsterdam, 1993), Vol. 7, and references therein.

[3] C.S. Wang, B.M. Klein, and H. Krakauer, Phys. Rev. Lett. **54**, 1852 (1985).

[4] V.L. Moruzzi, P.M. Marcus, K. Schwarz, and P. Mohn, Phys. Rev. B **34**, 1784 (1986).

[5] Y. Zhou, W. Zhang, L. Zhong, X. Nie, and D.-S. Wang, J. Magn. Magn. Mater. **167**, 136 (1997).

[6] T. Asada and S. Blügel, Phys. Rev. Lett. **79**, 507 (1997).

[7] S. Müller, P. Bayer, C. Reischl, K. Heinz, B. Feldmann, H. Zillgen, and M. Wuttig, Phys. Rev. Lett. **74**, 765 (1995).

[8] S. Müller, P. Bayer, A. Kinne, P. Schmailzl, and K. Heinz, Surf. Sci. **322**, 21 (1995).

[9] J. Thomassen, F. May, B. Feldmann, M. Wuttig, and H. Ibach, Phys. Rev. Lett. **69**, 3831 (1992).

[10] M. Wuttig and J. Thomassen, Surf. Sci. **282**, 237 (1993).

[11] Dongqi Li, M. Freitag, J. Pearson, Z.Q. Qiu, and S.D. Bader, Phys. Rev. Lett. **72**, 3112 (1994).

[12] R.D. Ellerbrock, A. Fuest, A. Schatz, W. Keune, and R.A. Brand, Phys. Rev. Lett. **74**, 3053 (1995).

[13] F. Baudelet, M.-T. Lin, W. Kuch, K. Meinel, B. Choi, C.M. Schneider, and J. Kirschner, Phys. Rev. B **51**, 12 563 (1995).

[14] M.-T. Lin, J. Shen, W. Kuch, H. Jenniches, M. Klaua, C.M. Schneider, and J. Kirschner, Phys. Rev. B **55**, 5886 (1997).

[15] W. B. Pearson, *A Handbook of Lattice Spacings and Structures of Metals and Alloys* (Pergamon, Oxford, 1964).

[16] A. Dittschar, M. Zharnikov, W. Kuch, M.-T. Lin, C.M. Schneider, and J. Kirschner, Phys. Rev. B **57**, R3209 (1998).

[17] J. B. Pendry, *Low Energy Electron Diffraction* (Academic, New York, 1974).

[18] M.-T. Lin, J. Shen, W. Kuch, H. Jenniches, M. Klaua, C.M. Schneider, and J. Kirschner, Surf. Sci. **410**, 290 (1998).

[19] M. Zharnikov, A. Dittschar, W. Kuch, C.M. Schneider, and J. Kirschner, Phys. Rev. Lett. **76**, 4620 (1996).

[20] M. Zharnikov, A. Dittschar, W. Kuch, C.M. Schneider, and J. Kirschner, J. Magn. Magn. Mater. **174**, 40 (1997).

[21] A. Dittschar, W. Kuch, M. Zharnikov, and C.M. Schneider, J. Magn. Magn. Mater. **212**, 307 (2000).

[22] H. Okamato, T.B. Massalski, L.J. Swartzendruber, and P.A. Beck, Bull. Alloy Phase Diagrams **5**, 592 (1984).

[23] D.D. Chambliss and K.E. Johnson, Surf. Sci. **313**, 215 (1994).

[24] J. Thomassen, B. Feldmann, and M. Wuttig, Surf. Sci. **264**, 406 (1992).
[25] A. Kirilyuk, J. Giergiel, J. Shen, and J. Kirschner, Phys. Rev. B **52**, R11 672 (1995).
[26] J. Giergiel, J. Kirschner, J. Landgraf, J. Shen, and J. Woltersdorf, Surf. Sci. **310**, 1 (1994).
[27] J. Giergiel, J. Shen, J. Woltersdorf, A. Kirilyuk, and J. Kirschner, Phys. Rev. B **52**, 8528 (1995).
[28] S.D. Bader, J. Magn. Magn. Mater. **100**, 440 (1991).
[29] P.M. Marcus, V.L. Moruzzi, and S.-L. Qiu, Phys. Rev. B **60**, 369 (1999).
[30] D.E. Fowler and J.V. Barth, Phys. Rev. B **53**, 5563 (1996).
[31] D. Sander, Rep. Prog. Phys. **62**, 809 (1999).